The Role of Subtropical Irreversible PV Mixing in the Zonal Mean Circulation Response to Global Warming–Like Thermal Forcing

JIAN LU

Pacific Northwest National Laboratory, Richland, Washington

LANTAO SUN

National Center for Atmospheric Research, Boulder, Colorado

YUTIAN WU

New York University, New York, New York

GANG CHEN

Department of Earth and Atmospheric Sciences, Cornell University, Ithaca, New York

(Manuscript received 27 June 2013, in final form 21 November 2013)

ABSTRACT

The atmospheric circulation response to the global warming–like tropical upper tropospheric heating is revisited using a dry atmospheric general circulation model (AGCM) in light of new diagnostics based on the concept of finite-amplitude wave activity (FAWA) on equivalent latitude. For a given tropical heating profile, the linear Wentzel–Kramers–Brillouin (WKB) wave refraction analysis sometimes gives a very different and even opposite prediction of the eddy momentum flux response to that of the actual full model simulation, exposing the limitation of the traditional linear approach in understanding the full dynamics of the atmospheric response under global warming. The implementation of the FAWA diagnostics reveals that in response to the upper tropospheric heating, effective diffusivity—a measure of the mixing efficiency—increases and advances upward and poleward in the subtropics and the resultant enhancement and the poleward encroachment of eddy potential vorticity mixing leads to a poleward displaced potential vorticity (PV) gradient peak in the upper troposphere. The anomalous eddy PV flux, in balance with the PV dissipation, gives rise to a poleward shift in the eddy-driven jet and eddy-driven mean meridional circulation. Sensitivity experiments show that these irreversible dissipation processes in the upper troposphere are robust, regardless of the width of the tropical heating.

1. Introduction

One of the most robust features in the atmospheric circulation response to increasing greenhouse gas (GHG) forcing might be the poleward displacement of the eddy-driven component of the zonal mean circulation, including the poleward shift of the westerly jet and Ferrel cell and the poleward expansion of the Hadley cell (HC). These large-scale features can impact profoundly the patterns of weather and the distributions of extreme precipitation and drought (Lorenz and DeWeaver 2007; Seager et al. 2007; Scheff and Frierson 2012). The mechanisms for the circulation response to global warming have been the topic of intensive research recently. A plethora of mechanisms has been proposed and most of the previous studies attributed these large-scale features to extratropical causes. For example, Lorenz and DeWeaver (2007) linked the poleward shift in zonal mean circulation to the rise of the extratropical tropopause, a feature that has been found to be effective in driving the jet shift in other independent studies (Haigh et al. 2005; Williams 2006). Lu et al. (2008) and Chen et al. (2008) further proposed that the increased meridional temperature gradient associated with the extratropical tropopause rise can lead to faster phase speeds of the baroclinic waves, which mostly end up

Corresponding author address: Jian Lu, 902 Battelle Boulevard, P.O. Box 999, MSIN K9-24, Richland, WA 99352.
E-mail: jian.lu@pnnl.gov

DOI: 10.1175/JCLI-D-13-00372.1

with breaking and absorption near the critical latitude where the wave phase speed approaches that of the background mean wind at the equatorward flank of the jet. Given that the mean wind in the subtropics increases poleward with latitude, faster phase speeds should correspond to more poleward critical latitudes and, accordingly, more poleward occurrence of wave breakings. As a consequence, the wave breaking–induced eddy momentum forcing will also shift poleward. Kidston et al. (2011) noticed a robust increase in the eddy length scale in anthropogenic climate change simulations. They further investigated the consequence on the eddy-driven jet and argued that an increase in the eddy length scale reduces its zonal phase speed relative to the background mean wind on the poleward flank of the jet and thus causes eddies to dissipate farther from the jet core. If the eddy dissipation region on the poleward flank of the jet overlaps with the eddy source region, shifting this dissipation to higher latitudes will alter the peak latitude of the eddy momentum forcing for the jet and hence the jet itself. Recently using a finite-amplitude wave activity (FAWA) budget, Chen et al. (2013) and Sun et al. (2013, hereafter SCL) also noticed a reduction of wave activity dissipation on the poleward flank of the jet in response to idealized climate change forcings. In contrast, this reduction is argued to allow more upward propagating baroclinic waves to move away from the latitude of baroclinic generation rather than to induce a change in poleward wave propagation.

On the other hand, the most pronounced feature associated with the jet shift and the HC expansion is an enhanced temperature warming in the upper tropical troposphere, likely resulting from the moist adiabatic adjustment to the tropical sea surface temperature (SST) warming. Accompanying the tropical upper tropospheric warming is an increase of dry static stability in the tropics. Dynamic scaling analysis (Lu et al. 2007, 2010; Frierson et al. 2007; Kang and Lu 2012) identified a strong linkage between the jet shift (and the HC expansion) and the increase of the tropical-to-subtropical static stability. Idealized modeling studies further substantiated the link of the upper tropospheric warming to the poleward shift of the jet and the HC edge. For example, Butler et al. (2010) investigated the response of the extratropical circulation to thermal forcings prescribed in the tropical upper troposphere and found poleward shift of the storm track and eddy-driven jet in all forcing cases, regardless of the meridional extent of the forcing. A similar lack of sensitivity to the width of the upper tropical heating was reproduced with a different dry AGCM (SCL). These results from the full eddying models are somewhat at odds with what the linear Wentzel–Kramers–Brillouin (WKB) theory might predict. From our experience with the familiar phenomenon El Niño, we have learned that a meridionally confined tropical tropospheric heating drives an equatorial enhancement of the subtropical jet, which should draw equatorward the critical latitude and the associated wave activity propagation, leading to an equatorward shift of the eddy momentum flux and eddy-driven jet (Chang 1995; Seager et al. 2003; Harnik et al. 2010). As far as the aspects of tropical upper tropospheric heating and the associated enhancement of the subtropical wind are concerned, linear wave refraction can hardly distinguish the difference between El Niño and global warming, as will be revealed in the linear quasigeostrophic (QG) analysis. This apparent conflict between the linear argument and the full nonlinear simulations motivates us to further investigate the mechanism of the extratropical circulation response to the global warming–like thermal forcing in light of the perspective of irreversible eddy mixing in a budget of wave activity generation and dissipation.

To facilitate the comprehension of this paper, let us first lay out the theoretical underpinning for the main diagnostic approach of the current investigation. Following Andrews et al. (1987, chapter 7), the QG dynamics governing the tendency of the zonal-mean wind anomaly $\Delta\overline{u}$ (i.e., the difference between the control and perturbed runs) in response to an arbitrary external heating can be expressed as

$$\left[\frac{\partial^2}{\partial y^2}+\frac{1}{\rho_0}\frac{\partial}{\partial z}\left(\rho_0\varepsilon\frac{\partial}{\partial z}\right)\right]\left(\frac{\partial\Delta\overline{u}}{\partial t}\right)=\frac{\partial^2}{\partial y^2}(\Delta\overline{v'q'}+\Delta\overline{X})-\frac{\partial^2}{\partial y\partial z}\left(\frac{f_0\overline{\mathcal{H}}}{d\theta_0/dz}\right), \quad (1)$$

where $\overline{v'q'}$, $\overline{X}$, and $\overline{\mathcal{H}}$ are the zonal-mean eddy QG potential vorticity (PV) flux, zonal mean friction, and the zonally symmetric thermal forcing, respectively, others following the conventional notation. The steady-state zonal wind change can be obtained by inverting the frictional damping of zonal wind with appropriate boundary conditions. Defining the direct response to the thermal forcing, $\Delta\overline{u}_H$, as the wind anomaly governed by

$$\left[\frac{\partial^2}{\partial y^2}+\frac{1}{\rho_0}\frac{\partial}{\partial z}\left(\rho_0\varepsilon\frac{\partial}{\partial z}\right)\right]\left(\frac{\partial\Delta\overline{u}_H}{\partial t}\right)=-\frac{\partial^2}{\partial y\partial z}\left(\frac{f_0\overline{\mathcal{H}}}{d\theta_0/dz}\right), \quad (2)$$

where $\Delta\overline{u}_H$ is the zonal mean zonal wind anomaly directly induced by the PV source due to the zonally symmetric diabatic heating through PV inversion (e.g., Ren et al. 2011), the eddy-induced component of the wind response (defined as $\Delta\overline{u}_E=\Delta\overline{u}-\Delta\overline{u}_H$) through the eddy feedback, $\Delta\overline{v'q'}$, can be further expressed by

$$\left[\frac{\partial^2}{\partial y^2}+\frac{1}{\rho_0}\frac{\partial}{\partial z}\left(\rho_0\varepsilon\frac{\partial}{\partial z}\right)\right]\left(\frac{\partial\Delta\overline{u}_E}{\partial t}\right)=\frac{\partial^2}{\partial y^2}(\Delta\overline{v'q'}). \quad (3)$$

With appropriate boundary conditions, both $\Delta\overline{u}_H$ and $\Delta\overline{u}_E$ can be solved if the right-hand side terms of the equations are known. Since the full eddying system is ultimately forced by the thermal forcing, in principle the eddy flux term on the right-hand side of (3) is the deterministic consequence of the thermal forcing. By corollary, a functional relationship might exist between $\Delta\overline{u}_H$ and $\Delta\overline{v'q'}$ and hence between $\Delta\overline{u}_H$ and $\Delta\overline{u}_E$ in a parameterizational sense. A simplest scenario might be that the eddy PV flux and the resultant eddy-driven wind response are largely controlled by the modified wave propagation characteristics due to $\Delta\overline{u}_H$, and previous studies have suggested this might be the case for the eddy-driven response to El Niño (Seager et al. 2003; Harnik et al. 2010). To test this scenario, one must first isolate the thermally direct response $\Delta\overline{u}_H$. For this purpose, in this study we will take a numerical approach by constructing an axisymmetric AGCM on the sphere, which deals with nonlinear Hadley cell dynamics without making the QG approximation (e.g., Kim and Lee 2001). The derived $\Delta\overline{u}_H$ is then inserted to a linear QG model to examine its impact on the characteristics of wave propagation in the altered medium. However, as will be demonstrated later (sections 4 and 5), for the response to the global warming–related tropical upper tropospheric forcing, eddy feedback cannot be simply explained by the linear wave refraction by the modified thermally direct wind; instead, the irreversible mixing of PV, which usually takes place during the saturation stage of baroclinic eddy life cycle, is essential to the final response of the poleward shift of the eddy-driven jet.

Our numerical approach will help separate the thermally direct component from the eddy-driven component in the full zonal mean circulation response, but it is not our intention to develop an eddy closure theory for the latter based on the information of the former. In the absence of viable eddy closure theory for the eddy PV flux, diagnostic analysis taking account of the irreversible effects of the eddy adjustment can still help shed light on the dynamical mechanism conceptually. To this end, we adopt a novel Eulerian–Lagrangian diagnostics for FAWA budget developed by Nakamura and collaborators (Nakamura and Zhu 2010; Nakamura and Solomon 2010) and apply it to the forced transient evolutions governed by (1) so as to explain the steady-state response. The upshot of this study is a revised conceptual depiction of the jet response to global warming–related tropical heating: the irreversible mixing in the subtropics, as a result of the stirring by baroclinic eddies, sharpens the PV gradient poleward. Additionally, our work underscores the challenge to understand the global warming–related atmosphere dynamic response, of which the change of the meridional structure of the irreversible mixing induced by the thermally driven zonal flow change is an integral part.

This is a companion paper to SCL, where the atmospheric circulation response and sensitivity to the patterns of tropical tropospheric thermal forcing were investigated using the same modeling and diagnostic approaches and the role of irreversible PV mixing in the upper troposphere was first identified to be crucial to the shift of the jet. Those who are interested in more technical details about the model configurations and the FAWA diagnostics should refer to SCL. Here we will focus on the tropical upper tropospheric warming, a signature temperature response of the greenhouse gas–forced change, and highlight the critical role of subtropical irreversible mixing in the jet latitude shift. The paper is organized as follows. We will first introduce the modeling tools and analysis methods in section 2. We will verify the results of Butler et al. (2010) and show that the upper tropical tropospheric heating, both narrow and broad, can indeed produce a poleward jet shift and expansion of the Hadley cell when the full effect of the eddies adjustment plays out (section 3). Note that for the single-jet configuration of the control state, both the jet shift and the expansion/contraction of the Hadley cell are predominantly forced by the eddy momentum flux: they are two facets of the same phenomenon, although they can differ in other jet configurations or in response to different climate forcings. Therefore, in the context of this study, we treat the mechanism for the jet shift to be the same as for the Hadley cell expansion/contraction. In section 4, aided by the axisymmetric model we will show that the linear wave refraction calculation based on the direct zonal wind response ($\Delta\overline{u}_H$) to tropical thermal forcings will always produce an equatorward enhancement of the eddy momentum convergence for all tropical upper tropospheric warming cases examined, epitomizing the limitation of the linear WKB theory in predicting the actual full response. In section 5, the FAWA diagnostics will be utilized for the exposition of the irreversible processes that lead to the full extratropical response. The main finding regarding the role of irreversible PV mixing from the wave activity budget is further corroborated by the analysis of the statistics of cyclonic wave breakings (CWB) versus anticyclonic wave breakings (AWB) in section 5c. We will discuss in section 6 the implications of this idealized modeling result in understanding the dynamics of the circulation change under global warming. Finally, the paper will conclude with a brief summary.

2. Models and analysis methods

a. Full AGCM and thermal forcing

The main modeling tool of this study is the Geophysical Fluid Dynamics Laboratory (GFDL) dry atmospheric dynamical core forced by a relaxation toward a given radiative equilibrium temperature profile and damped by Rayleigh damping in the planetary boundary layer. The detail of the model configuration was described in Held and Suarez (1994), and the radiative equilibrium temperature is specified as

$$T_{\mathrm{eq}}^{c}(p,\phi) = \max\left\{200\,\mathrm{K}, \left[315\,\mathrm{K} - \delta_y \boxed{\sin^2\phi} - \delta_z \log\left(\frac{p}{p_0}\right)\cos^2\phi\right]\left(\frac{p}{p_0}\right)^{\kappa}\right\}, \quad (4)$$

where $\delta_y = 60\,\mathrm{K}$ and $\delta_z = 10\,\mathrm{K}$. All the T_{eq} profiles including the thermal perturbations used in this study are hemispherically symmetric. All integrations are performed at the horizontal resolution of R30 (rhomboidal 30 spherical harmonic truncations) with 20 evenly spaced sigma levels in the vertical.

In the perturbation experiments, diabatic perturbation is introduced by modifying the equilibrium temperature in the tropical troposphere. The detailed description for the thermal perturbations is provided in SCL. Here we only briefly describe the heating profiles corresponding to tropical upper-tropospheric warming set (TUW) data, which are designed to mimic the tropical heating profiles used in Butler et al. (2010). A perturbation of the form $F(p)W(\phi, \phi_0)$ is added to the box term in (4). As the result, the total equilibrium temperature becomes

$$T_{\mathrm{eq}}^{p}(p,\phi) = \max\left\{200\,\mathrm{K}, \left[315\,\mathrm{K} - \delta_y \boxed{\sin^2\phi + F(p)W(\phi,\phi_0)} - \delta_z \log\left(\frac{p}{p_0}\right)\cos^2\phi\right]\left(\frac{p}{p_0}\right)^{\kappa}\right\}. \quad (5)$$

In (5), $F(p) = A\exp[-(p/p_s - 0.3)^2/2\times 0.11^2]$ defines the structure of tropical heating centered at the upper troposphere with A set to be -0.1438; $W(\phi, \phi_0) = 0.5\{1 - \tanh[(|\phi| - \phi_0)/\phi\delta]\}$ is a weighting function to specify the meridional extent of thermal perturbations, with ϕ_0 setting the boundary of the thermal perturbation and $\delta\phi = 5°$ controlling the sharpness of the boundary. To test the sensitivity of the response to the widths of the tropical heating, we vary ϕ_0 from 10° to 30° with an increment of 5°. See Figs. 1a–f for the structures of T_{eq} with $\phi_0 = 10°$ and 30°, respectively. Note that the net heating to the atmosphere increases with increasing width. Sensitivities to the model horizontal and vertical resolutions and the type of numerical diffusions were already discussed in SCL.

b. Zonally symmetric model

The zonally symmetric model of the GFDL dynamical core is constructed for two purposes. First, by comparing the full response from the zonally symmetric response to a same thermal forcing, one can cleanly separate the effect of the eddy feedbacks from the direct thermally forced response as in Kim and Lee (2001). Second, to examine the change of the propagation characteristics of the linear waves under WKB assumptions, one should not impose the wind change simulated by the full model because it already includes the effect of eddies. A better practice would be to isolate the thermally direct component of the response in the absence of the eddy feedbacks and use it to perturb the mean state. As the spatial structure of the direct thermally forced response in the zonally symmetric model remains qualitatively similar in time, we will use the equilibrated change for the diagnostic of the refractive index.

In the zonal symmetric configuration, only the zonal mean part (spectral zonal wavenumber 0) is integrated forward in time and the effect of eddies is added as a constant external forcing to the primitive equations. The eddy forcing is diagnosed as the negative tendency of applying the zonal mean fields to the governing equations and integrating forward by one time step. See Kushner and Polvani (2004) and SCL for more details on the construction of the zonally symmetric model and the computation of eddy forcing. The eddy forcing helps to reproduce the same mean state as the full model. This is important for the nonlinear axisymmetric Hadley cell response to thermal forcing, which can depend on the mean state of the atmosphere (e.g., Held and Hou 1980).

c. Large member ensemble transient runs

In addition to the 4000-day-long equilibrated experiments, for each of the thermal forcings of interest we also run 100-member ensembles of transient experiments wherein the forcing is abruptly turned on. The purpose of these transient experiments is to dissect the processes of the evolution from the initial control state to the new forced equilibrium. To form a 100-member ensemble, we first run the control experiment for 7000 days, and then from every 50th day of the last 5000 days

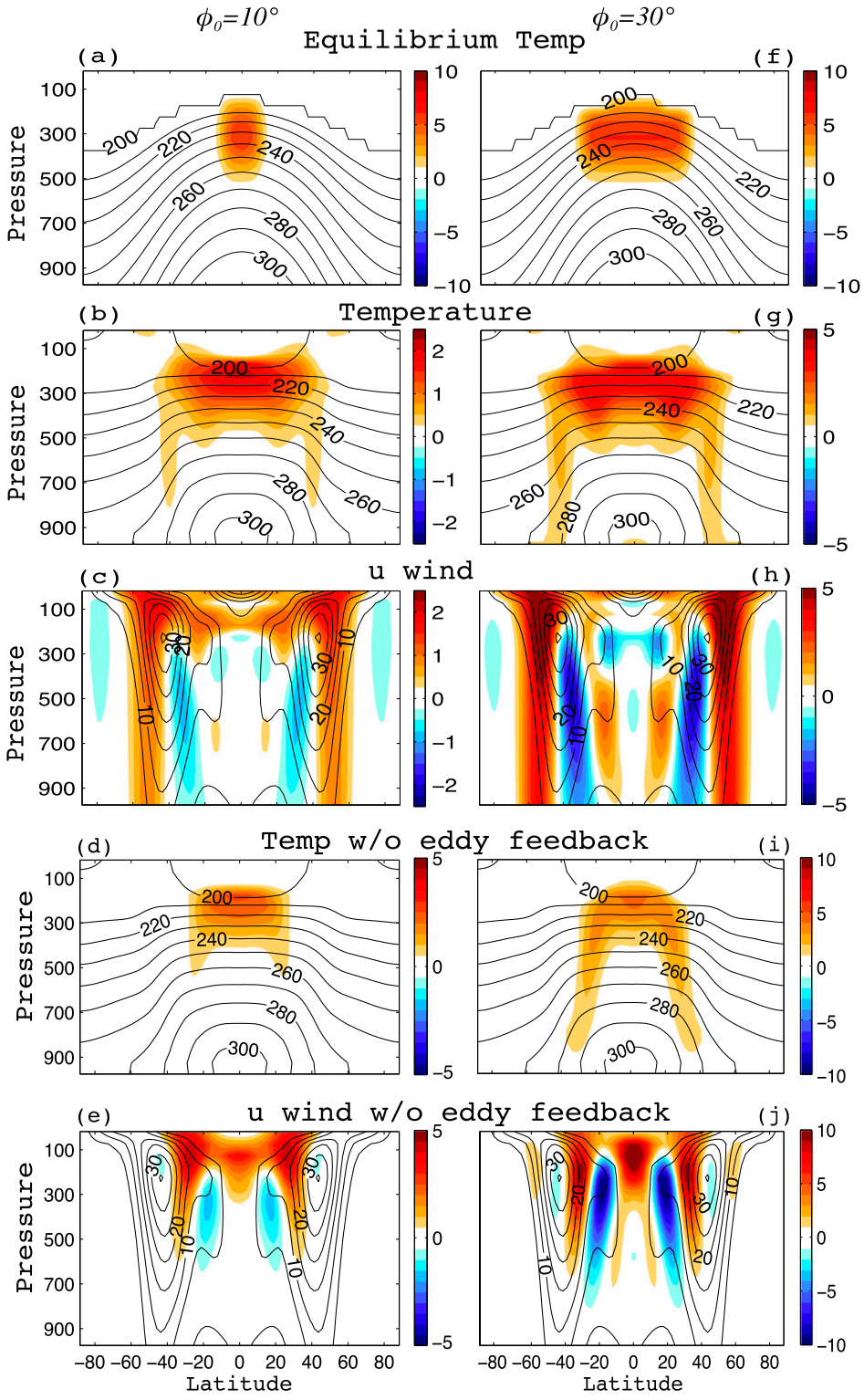

FIG. 1. The thermal forcing and response of the zonal mean temperature and zonal mean zonal wind in the full AGCM and the zonally symmetric model in (left) TUW10 and (right) TUW30 experiments. (a),(f) Equilibrium temperature; (b),(g) zonal mean temperature in full AGCM (K); (c),(h) zonal mean zonal wind in full AGCM ($m\,s^{-1}$); (d),(i) zonal mean temperature in the zonally symmetric model (K); and (e),(j): zonal mean zonal wind in the zonally symmetric model ($m\,s^{-1}$). In each panel, the climatological field is overlaid as contours.

a realization branches out. For each of the 100 realizations, the same thermal perturbation is switched on instantaneously and the model integrates for 200 days.

d. Refractive index diagnostics

The characteristics of linear waves propagating in a medium defined by the zonal mean background state are usually represented by the index of refraction, which is widely used in the dynamics community to understand the behavior of waves and their interaction with the mean flow (e.g., Charney and Drazin 1961; Matsuno 1970; Hoskins and Karoly 1981). The refractive index for a linearized QG PV equation in spherical coordinates for a disturbance with given zonal wavenumber s and frequency σ can be expressed as

$$n_{\rm ref}^2 = \frac{a\langle \overline{q}_\phi \rangle}{\langle \overline{u} \rangle - \dfrac{\sigma_r a \cos\phi}{s}} - \frac{s^2}{\cos^2\phi} + a^2 f^2 F(N^2), \quad (6)$$

where $\langle \overline{u} \rangle$ is the zonal mean wind, $\langle \overline{q}_\phi \rangle$ is the meridional gradient of zonal mean potential vorticity, σ_r is the real part of frequency, N is the Brunt–Väisälä frequency, and $F(N^2)$ is a function of N^2 (see Harnik and Lindzen 2001; Seager et al. 2003). Waves propagate in regions where $n_{\rm ref}^2 > 0$, are evanescent in regions where $n_{\rm ref}^2 < 0$, are reflected where $n_{\rm ref}^2 = 0$, and are absorbed where $n_{\rm ref}^2 \to \infty$. A general rule of thumb is that wave packets tend to refract toward large values of $n_{\rm ref}^2$ in regions of wave propagation.

While $n_{\rm ref}^2$ can be estimated directly from the given basic state and the properties of the wave, it includes the wave propagation characteristics in both meridional and vertical directions, yet only the meridional wavenumber is relevant for the eddy momentum flux and jet shift. Here we make use of a linear QG model to diagnose directly the wave propagation characteristics of a two-dimensional zonal mean basic state (Harnik and Lindzen 2001). The model takes as input the zonal mean zonal wind and temperature with a specified eddy angular phase speed and zonal wavenumber and solves the linearized QG PV equation with the eddy geopotential height perturbation specified at the surface. The model outputs the eddy fluxes, the index of refraction, and its separation into terms related to the squares of the vertical and meridional wavenumbers (m^2 and l^2, respectively):

$$m^2 + \frac{N^2}{f^2} l^2 = n_{\rm ref}^2 .$$

Studies have found that l^2 and m^2 from the linear QG solution serve better the purpose for indicating wave propagation in both the vertical and meridional directions than the direct estimation of $n_{\rm ref}^2$ (e.g., Harnik and Lindzen 2001; Perlwitz and Harnik 2003). Analogous to the effects of $n_{\rm ref}^2$, waves propagate (are evanescent) in the meridional direction in regions where $l^2 > 0$ ($l^2 < 0$), and the surface of $l^2 = 0$ ($l^2 \to \infty$) reflects (absorbs) the waves.

e. Finite-amplitude wave activity diagnostics

To elucidate the nonlinear aspects of the eddy–mean flow interaction in the extratropical circulation response to tropical forcings, we adopt the FAWA budget diagnostics developed by Nakamura and collaborators (Nakamura and Zhu 2010; Nakamura and Solomon 2010). While finite-amplitude pseudomomentum and pseudoenergy diagnostics have also been developed according to the generalized Lagrangian mean theory (e.g., Methven 2013), which better describes a local conservation of wave characteristics, Nakamura's formalism can better describe the eddy–zonal flow interaction and is thus more suitable for the purpose of the present study. In particular, the FAWA defined as (8) below satisfies the exact Eliassen–Palm (e.g., Andrews et al. 1987) and nonacceleration theorems

$$\frac{\partial A_L}{\partial t} + \overline{v'q'} = 0, \quad (7)$$

in the absence of friction and other nonconservative effects. Note that A_L in (7) measures the net areal displacement of the PV contours from zonal symmetry and is defined geometrically following the material surface of the QG PV as

$$A_L(p,\phi_e) \equiv \frac{1}{2\pi a \cos\phi_e}\left[\iint_{q>Q;\phi<\pi/2} q_{\rm QG}\, dS - \iint_{\phi_e<\phi<\pi/2} q_{\rm QG}\, dS\right]. \quad (8)$$

The equivalent latitude ϕ_e for a PV value Q (upper case is used to emphasize its Lagrangian property) is determined by the requirement that the area enclosed by the PV contour toward the polar cap equals the area poleward of ϕ_e, that is,

$$\iint_{q>Q;\phi<\pi/2} dS = \iint_{\phi_e<\phi<\pi/2} dS = 2\pi a^2(1-\sin\phi_e). \quad (9)$$

As such, a monotonic relationship between ϕ_e and Q may be established for each hemisphere and A_L is positive definite in the interior of the atmosphere. Moreover, a hybrid Eulerian–Lagrangian framework can be formulated for nonconservative flow as

$$\frac{\partial A_L}{\partial t} + \overline{v'q'} \approx -\frac{K_{\text{eff}}}{a}\frac{\partial Q}{\partial \phi_e} - \Delta\Sigma, \tag{10}$$

with the irreversible dissipation of wave activity expressed as downgradient PV diffusion. In (10) the eddy QG PV flux is a quantity in zonal average while others are Lagrangian quantities on equivalent latitudes. This, therefore, is an Eulerian–Lagrangian hybrid diagnostic system. Also, K_{eff} is the effective diffusivity of the irreversible mixing of tracers across material surfaces (e.g., Nakamura 1996) and can be calculated either as a residual using (10) or using the modified formula for the eighth-order hyperdiffusion used in our spectral model:

$$K_{\text{eff}} = \frac{\langle \kappa_{2m}(-1)^{m-1}\nabla[\nabla^{2(m-1)}q]\cdot\nabla q\rangle_Q}{\left(\frac{1}{a}\frac{\partial Q}{\partial \phi_e}\right)^2},$$

where $m = 4$, and $\langle\cdot\rangle_Q$ is an average near the PV contour Q (see appendix A in SCL for details). Here $\Delta\Sigma$ denotes the diabatic source/sink of wave activity at equivalent latitude and can be safely ignored in the transition behavior of interest here, which takes place long after the switch-on of the thermal forcing. It should be noted that the effective diffusivity accounts for both stirring due to the resolved advection processes and small-scale mixing that ultimately dissipates wave activity. While K_{eff} appears to be proportional to the numerical diffusivity κ_{2m} of the model, effective diffusivity is fundamentally governed by the large-scale stretching and deformation of PV contours. Therefore, K_{eff} is largely independent of the value of numerical diffusivity especially when the stirring scales are separable from the diffusion scales (e.g., Marshall et al. 2006).

Making use of (10), the budget for the QG EP flux divergence can be derived as

$$\frac{1}{a\cos\phi}\nabla\cdot\mathbf{F} = \overline{v'q'} \approx -\frac{\partial A_L}{\partial t} - \frac{K_{\text{eff}}}{a}\frac{\partial Q}{\partial \phi_e} - \Delta\Sigma. \tag{11}$$

This diagnostic equation relates the EP flux divergence/convergence, which serves as a source/sink for the zonal momentum in a transformed Eulerian mean (TEM) sense, to the wave activity tendency, the irreversible dissipation of wave activity, and the diabatic sink/source of wave activity. The leading-order balance in (11) will aid to reveal the key mechanisms for the eddy forcing for the shift of the eddy-driven circulation. Caution should be used in interpreting the budget within the deep tropics, where the QG approximations are no longer valid.

3. Equilibrium responses

A cursory survey of the full response to the TUW forcings indicates that the structures of the temperature and zonal wind response are all similar and the magnitude varies linearly with the width of the heating (see also SCL), so we shall mainly focus on the results of the narrowest ($\phi_0 = 10°$, referred to as TUW10 hereafter) and broadest ($\phi_0 = 30°$, referred to as TUW30 hereafter) cases of the group.

a. Full response

As reported in SCL, all the tropical upper tropospheric thermal forcings lead to a poleward displacement of the eddy-driven jet and a weakening and expansion of the Hadley overturning circulation. In addition, the magnitude of these features increases with the width of the tropical warming (see Fig. 3 in SCL). Figures 1b and 1g compare the full equilibrium temperature and zonal wind response between the narrowest (TUW10) and broadest (TUW30) cases of the TUW group. Despite the different widths of the heating source, the full temperature responses are similar in structure between the two cases: the warming is broadened by the dynamic adjustment in such a way that the meridional temperature gradients are enhanced near 35°–40° latitude at the level of heating; the warming bulges downward in both cases at around 20°, a latitude where the descending motion of the climatological overturning circulation is the strongest; the warming signal also extends downward to the lower troposphere near 40°–45°, largely resulting from the adiabatic warming associated with the anomalous eddy-driven downward motion there (not shown). Great similarity also exists in the zonal wind response between the TUW10 and TUW30 cases (Figs. 1c,h), both projecting strongly on the leading EOF pattern (i.e., the annular mode pattern) of the internal variability. The zonal wind response is in close thermal wind balance with the zonal mean temperature anomalies (Figs. 1c–h). The main difference between the two warming cases is more in magnitude than structure, implicative of a similar dynamical mechanism operating in both.

b. Axisymmetric response

Contrasting the axisymmetric temperature response (Figs. 1d,i) against the full response (Figs. 1b,g), one can see that some of the aforementioned features are rooted in the thermally direct response. The similar meridional spread of the warming between the narrow and broad cases reflects the key nature of the equatorial dynamics: the small Coriolis parameter there cannot maintain much temperature gradient and the Schneider–Held–Hou-type (Schneider 1977; Held and Hou 1980) Hadley

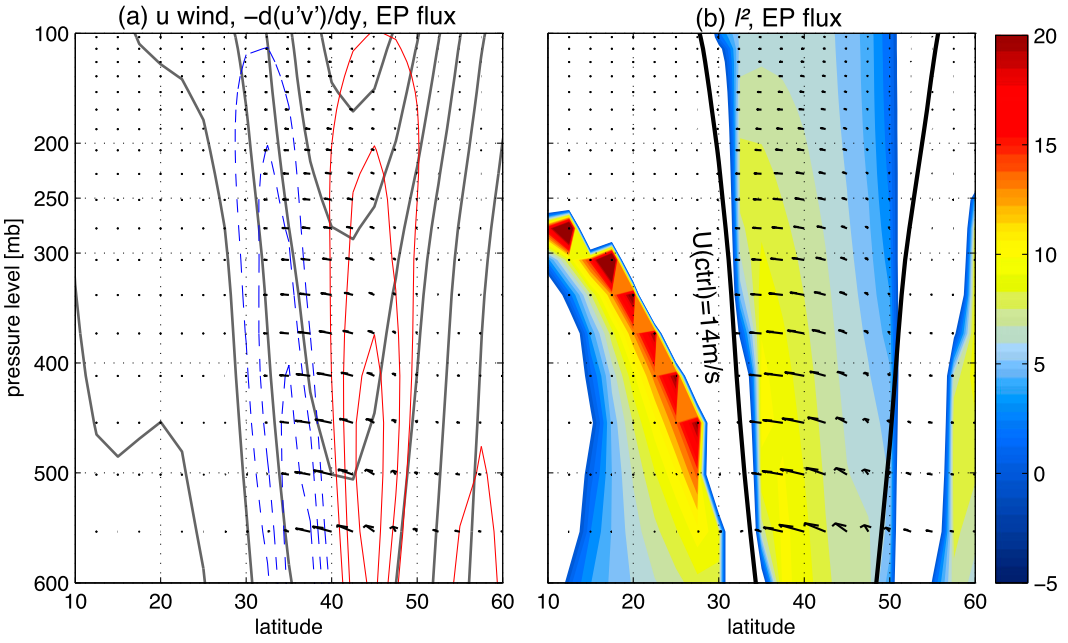

FIG. 2. Results of wave refractive index analysis for the control case. (a) Latitude–height plot of the zonal mean zonal wind (gray contours) and eddy momentum convergence (red and blue contours, respectively), and Eliassen–Palm (EP) flux (vectors) calculated from the linear QG wave refraction model. (b) Latitude–height distribution of the square of meridional wavenumber l^2 (shading, with the values <0 blanked out). The critical surfaces demarcated by the $U = 14\,\mathrm{m\,s^{-1}}$ isotach are also displayed as thick black lines. Note that wave amplitudes and correspondingly the magnitudes of eddy fluxes and convergence are arbitrary in the linear QG model.

cell adjustment always fixates the forced temperature gradient at the edge of the tropics (see also Satoh 1994). In the absence of eddy adjustment, the subtropical maximum warming at levels below the thermal forcing is now more conspicuous, stretching downward and poleward between 20° and 40° along the descending motion of the Lagrangian or TEM tropical overturning circulation (e.g., Tanaka et al. 2004). The zonal wind response in the axisymmetric model is in close thermal wind balance with the temperature field and is also very similar in structure between the narrow and broad warming cases, both characteristic of a tilted dipole between 15° and 40° latitudes (Figs. 1e,j). Note that in the absence of eddy feedback, an upper tropospheric thermal forcing produces little impact on the surface wind. These wind and temperature anomalies in the axisymmetric runs will next be used to perturb the background fields in the wave refractive index analysis.

4. Linear wave refraction analysis

Figure 2 shows the Eliassen–Palm (EP) flux and the convergence of eddy momentum flux (Fig. 2a) and the square of the meridional wavenumber (l^2; Fig. 2b) in the upper troposphere diagnosed from the linear QG PV model. They are the results of the specification of a wave source of wavenumber 6 and constant angular phase speed $3.1 \times 10^{-6}\,\mathrm{s^{-1}}$ (corresponding to linear phase speed of $14\,\mathrm{m\,s^{-1}}$ at 45° latitude) at the surface boundary, and the propagation is solely controlled by the specified basic state. Consistent with the typical EP flux in observations, the EP flux diagnosed from the refractive index analysis veers equatorward, pointing toward higher values of l^2. The critical surfaces where the background wind equals the phase speed (which is set to be $14\,\mathrm{m\,s^{-1}}$) are also displayed as black lines in Fig. 2b. One can see that the linear wave propagation is confined within the two critical surfaces with little wave activity leaking through the subtropical critical surface. This distribution of l^2 is somewhat different from what is considered in Seager et al. (2003) wherein the refractive index consists of two waveguides centered at 40° and 25°, respectively. The equatorward waveguide is associated with the thermally forced component of the subtropical jet, which is too weak in our control case compared to the observed counterpart, as commonly found in dry models without explicit convection (see the gray contours in Fig. 2a). Configured as such, the wave refraction is totally dictated by the specified mean flow and temperature with no feedback on the mean flow from the implied eddy fluxes. Therefore, even though the refraction-induced momentum convergence/divergence

is characterized by a dipole, the related westerly acceleration does not align with the location of the mean eddy-driven jet, implicative of the potential deficiency of the linear approach.[1]

When the control mean zonal wind and temperature are perturbed by the axisymmetric response to the TUW10 heating, the enhanced upper-level subtropical wind pushes the critical surface equatorward. The sharp increase of l^2 near the critical surface is the result of the equatorward expansion of the propagation zone. Within the propagation zone, the l^2 anomalies are characteristic of a tripole with two positive anomalies sandwiching a negative anomaly near 40°. This tripole guides the anomalous wave activity flux to diverge from the negative l^2 anomaly near 40° toward the positive l^2 anomalies on its both flanks (Fig. 3a). The eddy momentum convergence induced by the anomalous EP flux is more characteristic of a dipole, with an acceleration between the mean subtropical critical surface and the position of the climatological mean jet and a deceleration equatorward of the critical surface (Fig. 3c). The enhanced poleward propagation of waves also leads to a deceleration poleward of the mean jet, but much weaker in magnitude. Compared with the structure of the direct wind response (Fig. 1e), the eddy momentum feedback from the linear refraction acts to spread the initial thermally direct wind anomalies slightly poleward. However, the associated acceleration still takes place at the equatorward side of the climatological mean jet, and thus an equatorward enhancement of the total wind (i.e., the thermally direct wind plus the eddy feedback wind) would be anticipated from the linear wave refraction feedback. For the broad tropospheric warming case (TUW30), despite the 20° difference in the meridional breadth of the forcing, the response in l^2 (Fig. 3b) and the associated change in eddy momentum convergence (Fig. 3d) resemble remarkably in structure their narrow counterparts, likely due to the mediating effect of the Schneider–Held–Hou-type adjustment. Despite the different basic state and tropical thermal forcing considered here, our result suggests a similar linear mechanism to what has been examined by Seager et al. (2003) and Harnik et al. (2010) for the El Niño condition.

Through a similar QG calculation, Harnik et al. (2010) were able to produce the patterns of the eddy-induced acceleration and deceleration in the subtropics through midlatitudes that match well with the tendencies of the zonal mean flow anomaly in the full model in response to El Niño forcing. However, from the antecedent discussion one can see that the linear wave refraction feedbacks under the TUW-type heating both produce equatorward enhancement of eddy driving, contradicting directly the poleward shift of the midlatitude circulation simulated by the full model. This stark contrast between the linear QG analysis and full nonlinear simulations calls into question the sufficiency of the former in guiding our understanding of the role of the eddy feedback in the midlatitude circulation response. As to be shown later in the transient adjustments, while the linear wave refraction analysis is still useful for indicating the instantaneous feedback from the eddies caused by the modified mean flow, it falls short in representing the irreversible aspects of the full eddy adjustment, a topic of the following section.

[1] The eddy momentum convergence diagnosed from the full model output does align well with the eddy-driven jet near 43°.

5. Transient responses to narrow versus broad upper-tropospheric tropical warming

a. Zonal wind and eddy momentum flux convergence

It is clear from the linear QG wave refraction analysis above that the full response of the circulation to tropical upper-tropospheric warming cannot be explained by the altered wave propagation characteristics resulting from the thermally direct part of the change of the mean wind. To elucidate the irreversible processes of the eddy adjustment that lead up to the full response, for both the TUW10 and TUW30 cases, we conduct 100-member ensemble simulations. Given the interhemispherical symmetry in a statistical sense, the Southern Hemisphere data are reflected about the equator to the Northern Hemisphere so as to double the sampling size. Therefore, all the ensemble mean results presented below are based on an ensemble size of 200.

Figures 4a–d show the evolution of the anomalous zonal wind at 875-hPa level in the transient ensemble experiments with the full model for the TUW10 and TUW30 warming cases, respectively. Owing to the vibrant internal variability of the midlatitude winds, the ensemble mean signal is still noisy. This is especially true for the case of the narrow warming wherein the forced signal is weak and subject to the disruption of internal noise. Nevertheless, the transitional behavior of the forced response from an equatorward to a poleward westerly enhancement is clearly discernable. It is also clear that this transition is directly forced by the poleward migrating eddy momentum convergence, with the eddy forcing leading the wind by approximately 5 days. The lead–lag relationship between the phases of the eddy momentum forcing and the near-surface zonal wind is clearer when both are projected onto the leading EOF pattern (i.e., the annular mode or zonal index) of

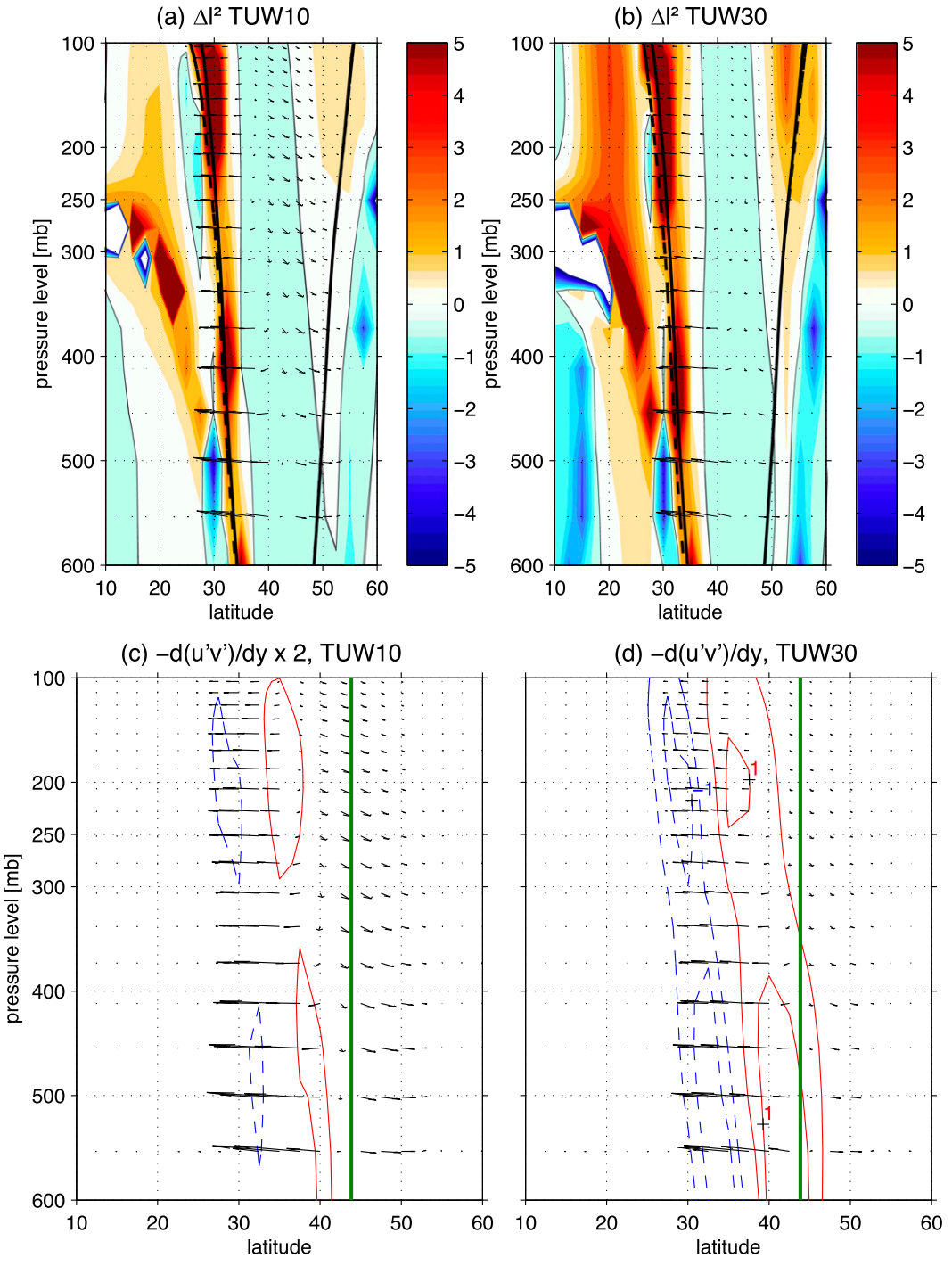

FIG. 3. (a),(b) The change of the square of meridional wavenumber l^2 (shading) because of the zonally symmetric response to TUW10 and TUW30 forcings. The critical surfaces denoted by the $U = 14\,\mathrm{m\,s^{-1}}$ isotach are also displayed as thick black lines for the control (solid) and perturbation (dashed) runs. (c),(d) The corresponding changes of eddy momentum convergence (red contours) and divergence (blue contours) and EP flux (vectors) under the forcing of TUW10 and TUW30, respectively. The green lines in (c) and (d) indicate the latitude of the climatological mean jet. Note that the magnitude of the wave quantities is arbitrary in the linear QG model.

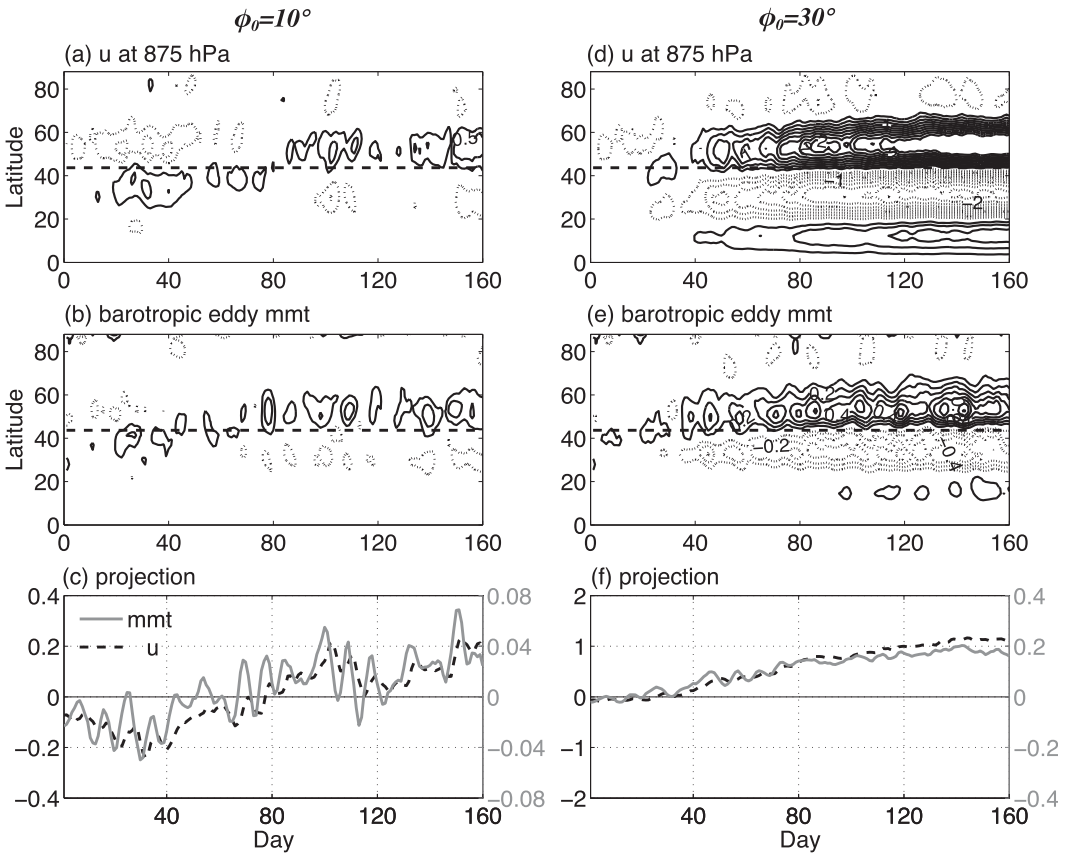

FIG. 4. (a),(d) The transient evolutions of zonal-mean zonal wind anomalies at 875 hPa in the (left) TUW10 and (right) TUW30 experiments. Contour interval is 0.25 m s^{-1} with the zero contours omitted. (b),(e) As in (a),(d), but for the barotropic momentum convergence anomaly. The black dashed lines in the top and middle panels denote the latitude of the climatological jet. Contour interval is 0.1 m s^{-1} day^{-1}. (c),(f) As in (a),(d), but for the projections of the 875-hPa zonal wind and eddy momentum convergence onto the leading EOF of 875-hPa zonal wind. Note that the scales of the *y* axis are different by a factor of 5 between (c) and (f).

the 875-hPa wind of the control run (Figs. 4c,f). Although no obvious equatorward-to-poleward transition is found in the transient response to the TUW30 forcing, the initial zonal wind response is still characteristic of a weak equatorward enhancement, consistent with the linear wave refraction analysis. By the end of the transient run, the broad warming produces about 5 times as large a shift as the narrow warming. Note that the scale of the projection onto the annular mode for the broad warming case is 5 times as large as that for the narrow warming case.

For the El Niño case, Harnik et al. (2010) applied the linear wave refraction analysis to all the instants of the zonal wind evolution in the ensemble response to a sudden switch-on of the El Niño forcing. They found that the poleward spread of the wind anomalies with time can be accounted for by linear wave refraction and the final equilibrium state is maintained by the wave–mean flow interaction system, of which the linear wave refraction feedback is a central part. To see if this is also the case for the TUW30 case here, we follow their approach and perform the same wave refraction analysis for every day of the 160 days of the ensemble mean wind response. The resultant eddy momentum acceleration/deceleration at upper-level troposphere between day 10 and 60 is displayed in Fig. 5b to compare with the corresponding level of full zonal wind (Fig. 5a) and full eddy momentum forcing (Fig. 5c). A very similar calculation was also performed for the transient zonal wind evolution in the National Center for Atmospheric Research (NCAR) Community Atmospheric Model, version 3 (CAM3), coupled to a slab ocean model to an instantaneous doubling of CO_2 (Wu et al. 2012, 2013). Consistent with the notion of Harnik et al. (2010), the linear wave refraction feedback acts to sustain the zonal wind anomalies that favor it. In addition, it contributes to the eddy–mean flow interaction that maintains the shifted jet at equilibrium. What is at issue is whether

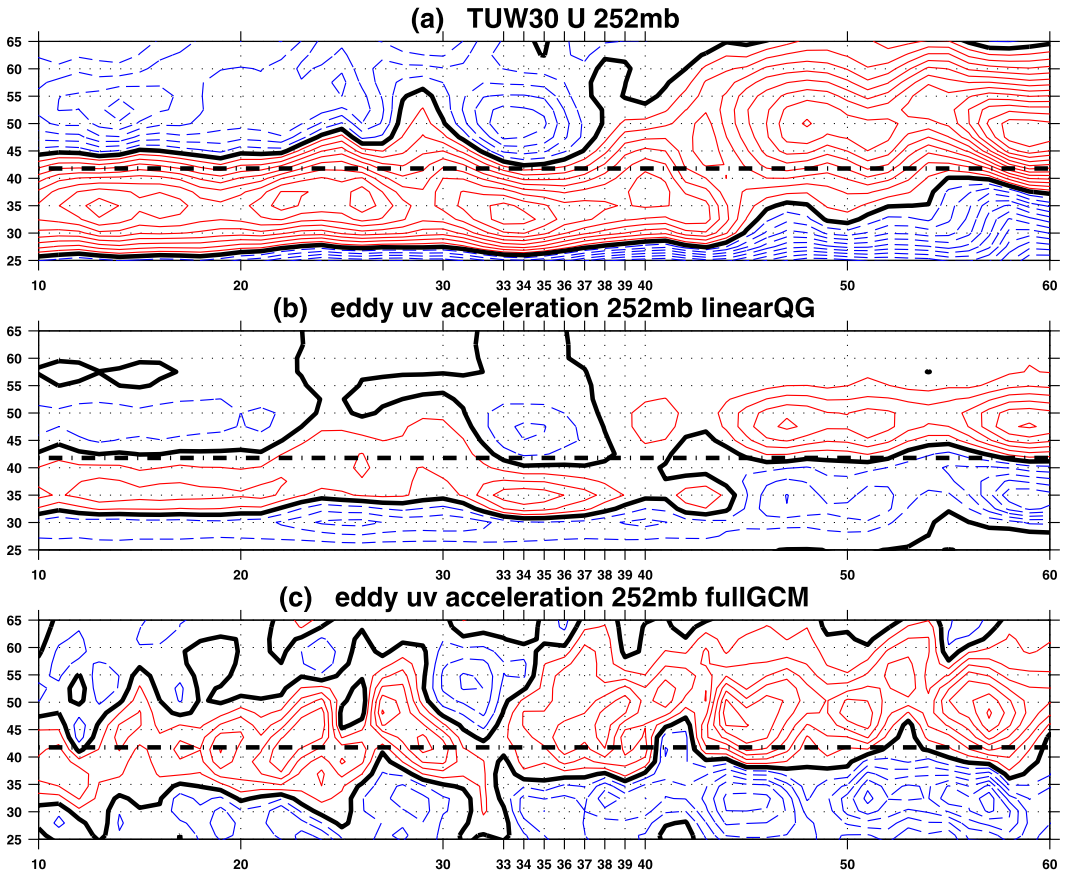

FIG. 5. The ensemble mean evolution under the TUW30 thermal forcing of (a) 252-mb zonal wind, (b) eddy momentum convergence from linear QG analysis, and (c) eddy momentum convergence produced in the full ensemble simulation. Only the period centered around the poleward transition of the eddy driven jet is shown. The black dashed line denotes the location of the climatological jet. Contour intervals are 0.1 m s^{-1} and 0.1 m s^{-1} day^{-1} in (a) and (c), respectively, and arbitrary in (b).

the linear wave refraction mechanism is responsible for instigating the eddy momentum forcing for the poleward transition of the jet. Comparing the temporal evolution of the acceleration in Figs. 5b and 5c against that of the zonal wind, we see that it is the full acceleration that leads the zonal wind, whereas the linear wave feedback is largely in phase with the zonal wind itself, with a few occasions when the former even lags the latter. In particular, during the transition time (from day 33 to 43), the burst of eddy momentum acceleration directly responsible for the poleward migration of the 252-hPa zonal wind takes place largely without the contribution from the linear refraction feedback. Based on this evidence, we can only conclude that linear wave refraction mechanism, in the absence of the change of the wave speed and/or wave length, only plays a feedback role in sustaining the wind anomalies that already exist, and falls short in serving as the initiating mechanism for the poleward transition of the jet.

b. Irreversible eddy mixing through finite-amplitude wave activity diagnostics

Before delving into the FAWA analysis, let us first examine the temporal evolutions of EP flux in the two TUW ensemble experiments. For reference, Fig. 6a gives the climatological EP flux (vectors) and divergence (shading), together with the momentum convergence (contours). Guided by the temporal evolution of the near-surface wind and the barotropic eddy momentum forcing (Figs. 4c,f), we divide the evolution of the transient wind response into two stages—the stage prior to the shift (before day 38) and the stage of shifted jet (around day 100)—and plot the trends of the EP flux accordingly for both ensemble experiments. The most pronounced features in the EP flux divergence during the preshift stage are the reduction (red color) of the climatological convergence centered at 350 hPa and 45° latitude and the enhancement (blue color) of convergence

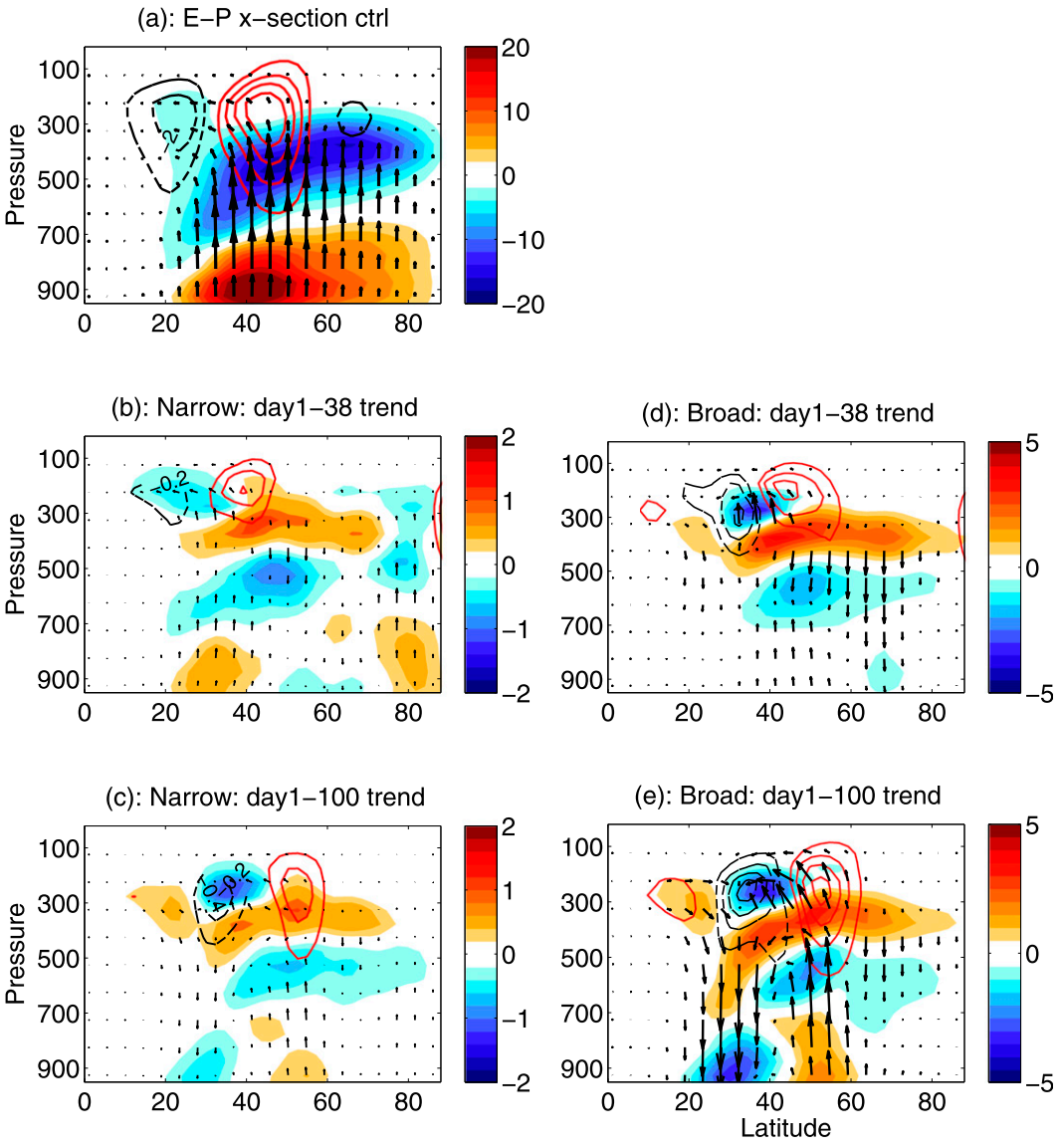

FIG. 6. (a) Climatological EP flux vector, EP flux divergence ($m\,s^{-1}\,day^{-1}$; shading), and eddy momentum convergence (contours) in the control experiment. The red solid contours denote the positive eddy momentum convergence and the black dashed contours the negative convergence. (b),(c) As in (a), but for the ensemble mean trend from day 1 to 38 and from day 1 to 100, respectively, in the transient experiments under TUW10 warming. (d),(e): As in (b),(c), but for TUW30 warming. The contour intervals are $1\,m\,s^{-1}\,day^{-1}$ in (a), $0.2\,m\,s^{-1}\,day^{-1}$ in (b) and (c), and $0.5\,m\,s^{-1}\,day^{-1}$ in (d) and (e). Zero contours for eddy momentum convergence are omitted.

at its equatorward and upward side (Figs. 6b,d). A similar dipole is evident in both the narrow and broad heating cases, with the latter being slightly poleward displaced. As will be explained later, the positive EP flux divergence in the upper troposphere is the result of reduced dissipation of wave activities coming from below and those that survive can reach the level of free propagation and propagate meridionally.

Extending the trend analysis to day 100 indicates that similar EP flux and convergence patterns progress gradually poleward with time and result in very similar patterns of EP flux and eddy momentum convergence for both heating cases (Figs. 6c,e). Now the eddy momentum convergence and divergence are located at 55° and 35° respectively with the nodal point at 43°, a perfect pattern for the poleward shift of the eddy-driven jet. Accompanying this poleward progression of the EP flux divergence dipole is the anomalous upward (downward) EP flux in the mid-to-lower troposphere at the poleward (equatorward) flank of the mean eddy-driven jet, consistent

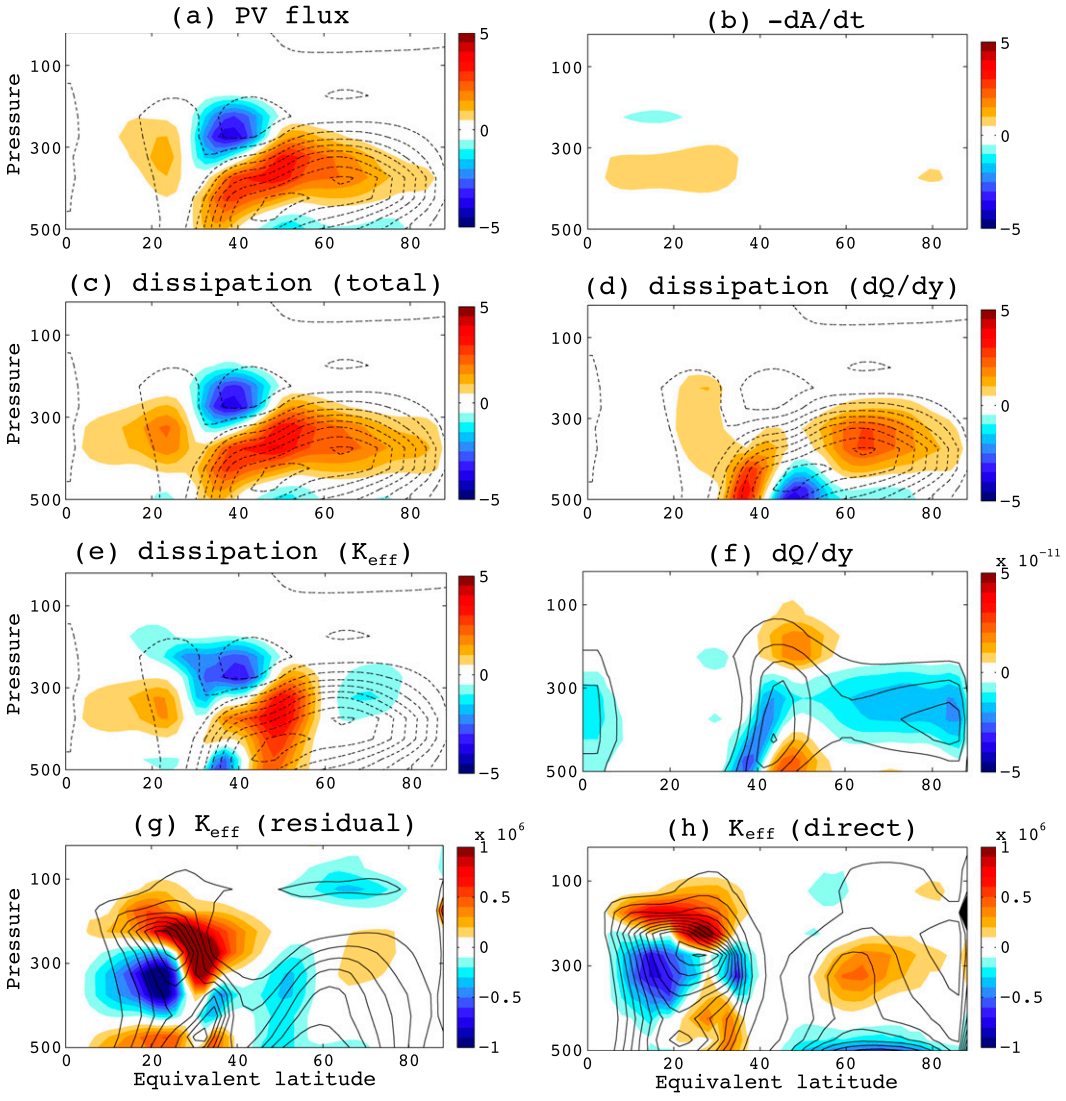

FIG. 7. The linear trend of the ensemble mean wave activity budget [see (8)] from day 1 to 100 in the TUW30 simulation. (a) Eddy PV flux, (b) negative wave activity tendency, (c) total dissipation change, (d) dissipation change because of PV gradient change, (e) dissipation change because of effective diffusivity change, (f) PV gradient change, (g) effective diffusivity change derived as residual, and (h) directly estimated effective diffusivity change. The contours in (a),(c),(d),(e) are the climatological mean PV flux. The contours in (f)–(h) are the corresponding climatological fields. The contour intervals for the climatological eddy PV flux, PV gradient, and effective diffusivity are $2\,\mathrm{m\,s^{-1}\,day^{-1}}$, $4.0 \times 10^{-11}\,\mathrm{m^{-1}\,s^{-1}}$, and $4.0 \times 10^{5}\,\mathrm{m^{2}\,s^{-1}}$, respectively.

with the poleward transition of the lower-level baroclinicity represented by the maximum Eady growth rate (not shown). These low-level EP flux anomalies should be interpreted as the positive feedback (through the altered baroclinicity) to, rather than the cause for, the poleward shift of the eddy-driven jet. Similar baroclinic feedback was also noticed in the transient response to the TUW30 heating in SCL and in the aquaplanet model simulation in Chen et al. (2013). As will be demonstrated next, the evolution of the anomalous EP flux and the associated wind response can be accounted for largely by the upper-level dissipation processes.

In view of that the EP flux adjustment during the period (days 1–100) of the poleward shift is characteristically the same between the TUW10 and TUW30 cases, we only show the FAWA budget for the TUW30 case in Fig. 7. The results for TUW10 only differ in magnitude and hence are not shown. The wave activity tendency (Fig. 7b) and the diabatic source (not shown) terms during days 1–100 turn out to be small and the

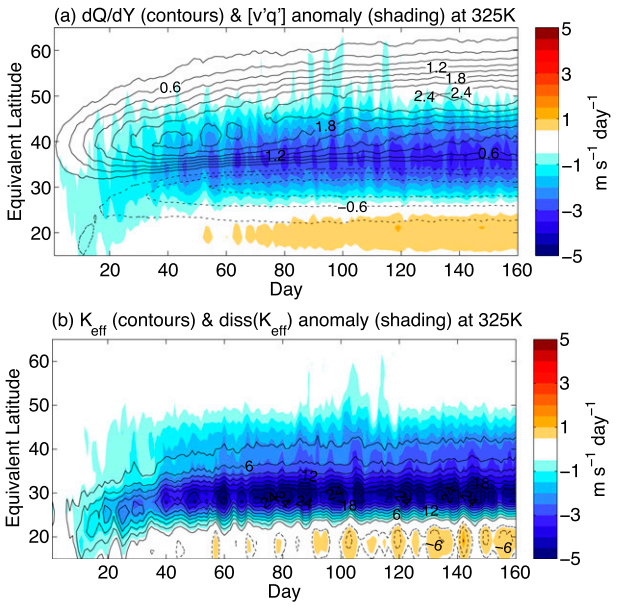

FIG. 8. The response to TUW30 warming as a function of time and equivalent latitude. (a) Contours of the meridional gradient of the Lagrangian PV at 325 K (contour interval is 1.0×10^{-11} m^{-1} s^{-1}). Shadings indicate the eddy PV flux at 325 K. (b) Contours of the anomalous K_{eff} (contour interval is 1.0×10^{5} m^{2} s^{-1}). Shadings indicate the dissipation component resulting from the change of K_{eff}.

main balance is between the PV flux trend (Fig. 7a) and the trend of the dissipation of wave activity (Fig. 7c). The dissipation term can be further decomposed into the components of PV gradient change (Fig. 7d) and effective diffusivity change (Fig. 7e), that is,

$$-\delta\left[\frac{K_{\text{eff}}}{a}\frac{\partial Q}{\partial \phi_e}\right] \approx -\frac{K_{\text{eff}}}{a}\delta\left[\frac{\partial Q}{\partial \phi_e}\right] - \delta K_{\text{eff}}\frac{\partial Q}{a\partial \phi_e}. \qquad (12)$$

The PV gradient and its change can be directly computed in equivalent latitude and the results are shown in Fig. 7f. In the upper troposphere, the maximum of the climatological PV gradient is located at 43° latitude, in alignment with the minimum of diffusivity and the position of the mean westerly jet. As such, the westerly jet acts as a mixing barrier in the upper troposphere in the same sense as does the core of the Antarctic Circumpolar Current in the Southern Ocean (Marshall et al. 2006; Ferrari and Nikurashin 2010). Under the TUW30 forcing, the total PV gradient is overall weakened except for a strengthening near the tropopause slightly poleward of the mean maximum. This poleward enhancement of the PV gradient (see also Fig. 8a) is consistent with what is found in the similar experiment conducted with a different AGCM by Butler et al. (2011, see their Fig. 7a), but with a key difference here that the enhancement of PV gradient contributes marginally to change of dissipation as it coincides with the climatological diffusivity minimum (cf. Fig. 8d).

The dissipation features that matter most for the eddy momentum flux arise from the change of effective diffusivity. In particular, the enhancement (reduction) of dissipation centered at 40° and 250 hPa (50° and 400 hPa) plays the dominant role in anchoring the upward and equatorward EP flux and maintaining a poleward transport of momentum (cf. Fig. 6e). The change of effective diffusivity is also responsible for most of the subtropical PV flux anomalies, which in turn are related to the weak eddy-induced momentum acceleration near 15° and 300 hPa (Fig. 6e). This, together with the deceleration farther poleward, represents a poleward advance of the critical layer where the subtropical wave breaking usually occurs and the wave activity gets dissipated. Speculatively, critical layer feedback through the increased phase speed of waves might be involved in the subtropical adjustment (e.g., Chen et al. 2008).

The change of the K_{eff} inferred from (11) as a residual is shown in Fig. 7g. It is this pattern of K_{eff} change, acting on the background PV gradient, that accounts for most of the dissipation change in the subtropics and midlatitude (Fig. 7e). The most prominent feature in Fig. 7g is a dipole in the subtropics with a decrease centered at 20° (350 hPa) and an increase at 30° (250 hPa). Adding onto the background mean K_{eff}, this dipole tends to shift the center of the total effective diffusivity poleward and slightly upward. A special note of caution should be added that this residual estimate of K_{eff} cannot be guaranteed to be accurate given the many assumptions made in the budget. Perhaps the most critical caveat of the diagnostics above is the assumption that (11) is balanced to a good approximation, which is not guaranteed given the QG approximations. As an a posteriori cross-validation, we directly compute K_{eff} making use of the formula of Nakamura and Zhu (2010) for an arbitrary tracer satisfying the advection–diffusion equation (see the appendix of SCL). The result is presented in Fig. 7h. Although the pixel-to-pixel match is elusive, the qualitative agreement between the direct estimate and the residual estimate is encouraging. Most importantly, the up-and-poleward enhancement of the mixing in the subtropical upper troposphere identified above can be reasonably vindicated by the direct estimate. It follows that the insights gained from the wave activity budget above are likely to hold for the response in question, and are not susceptible to errors because of the QG approximations.

In summary, we find that the enhancement and poleward advance of the upper-level mixing is key for the equilibrating of the eddy PV flux, a somewhat different assertion from Butler et al. (2011), who argued that the thermally forced PV gradient anomalies dictate the eddy

adjustment. To compare with Butler et al. (2011), Fig. 8a shows the temporal evolution of the ensemble mean QG PV flux and Lagrangian PV gradient (dQ/dy) interpolated onto the isentropic surface near the tropopause (325 K). Qualitatively the same evolution has been derived with the direct calculation of the isentropic eddy Ertel PV flux and hence is not shown. This approach can be justified by the fact that the meridional eddy QG PV flux is a good approximation for the residual eddy Ertel PV flux in the QG limit (Plumb and Ferrari 2005). Near the tropopause level, although the anomalous PV gradient (contours in Fig. 8a) exhibits a similar dipolar structure to that of the experiment in Butler et al. (cf. their Fig. 7a), the eddy PV flux anomalies are not exactly down the anomalous PV gradient as in Butler et al. (2011) (cf. our Fig. 8a and their Fig. 7a). Instead, as shown in Fig. 8b, during the adjustment toward the equilibrium the effective diffusivity (contours) gradually strengthens and advances poleward, a process that dominates the total change of the dissipation term and hence the eddy PV flux (cf. the shading in Figs. 8a and 8b). Our result suggests that the simple depiction of the downgradient eddy PV flux put forward by Butler et al. (2011; see schematic in their Fig. 8), while valid for the particular case investigated therein, may not be adequate for portraying the full irreversible processes important for the adjustment of the midlatitude circulation to a tropical thermal forcing in general. Our result also underscores the challenge of understanding the atmospheric circulation response under global warming: for a theory to predict the response of the eddy-driven wind, it must also predict the change of the effective diffusivity.

What drives the change in effective diffusivity? Simple models of transport and mixing have suggested that a stronger zonal jet tends to reduce the effective diffusivity across the jet, leading to a stronger transport barrier (Haynes et al. 2007). The initial change (from day 1 to 30) in our switch-on transient simulations, as well as the zonally symmetric model, shows a strengthening of zonal wind (Figs. 1e,j and 5a) or PV gradient (Fig. 8a) on the equatorward side of the mean jet. In the full model, however, we see that the effective diffusivity enhancement drifts from 15°–30° to 20°–35° during the first 40 days (Fig. 8b). Since the effective diffusivity has increased against the suppression by a stronger thermally driven subtropical jet, eddy stirring has to increase at the latitudes of 30°–35° so as to break the mixing barrier that is reinforced initially by thermal forcing. This latitudinal shift in eddy stirring may be explained by a change in wave characteristics or an increased equatorward wave propagation resulting from either less poleward wave propagation (Kidston et al. 2011; Lorenz 2013, manuscript submitted to *J. Atmos. Sci.*) or less local dissipation at the latitude of baroclinic wave generation (Chen et al. 2013; SCL). The latter is supported by an increase in wave activity amplitude prior to the poleward transition in jet latitude (not shown). It would probably require a space and time decomposition of wave activity to understand why the stirring in subtropics is increased, which is beyond the scope of this study. Nevertheless, we have demonstrated that effective diffusivity can quantify the efficiency of the irreversible mixing of PV in understanding the jet shift, a capability beyond the traditional Eulerian diagnostics.

c. *Wave breaking statistics*

The effective diffusivity diagnosed above reflects the mixing in a coarse-grain sense due to the chaotic advection or stirring by the resolved flow fields, which produce increasingly finer scales in the PV distribution until the small-scale dissipation takes over (e.g., Haynes and Shuckburgh 2000). In the upper troposphere, strong chaotic stirring and the resultant irreversible mixing take place where synoptic wave breaking events occur, usually at the flanks of the jet near critical latitudes. The jet, on the other hand, acts as a barrier for mixing. As such, there might exist a good correspondence between the statistics of wave breakings and the distribution of effective diffusivity. Further evidence for the notion above about the importance of changing effective diffusivity may be collected from the changing statistics of the wave breaking events.

To obtain the statistics of wave breaking, we make use of the wave breaking detection algorithm of Rivière (2009) to detect the grid points where a local reversal of the QG PV takes place. The grid point occupied by a cyclonically (anticyclonically) overturning PV filament is identified as a cyclonic (anticyclonic) wave-breaking region and is denoted as CWB (AWB). Figure 9a shows the total frequency of the AWB (solid contours) and CWB (dashed contours) from the long control experiment, measured by the fraction of the meridians subject to wave breaking for a latitudinal circle in a time average sense. Comparing to the contours in Fig. 7g, it is clear that the subtropical section of the large effective diffusivity results predominantly from the AWB and the midlatitude section from the CWB, respectively. Notably, the linear trend of the wave breaking statistics in the ensemble adjustment to the TUW30 forcing (Fig. 9b) bears a qualitative resemblance to the trend of K_{eff} and thus these two fields are connected: the subtropical dipole in AWB frequency implicates an upward and poleward increase of the wave breaking–related effective diffusivity near the tropopause level; meanwhile, the decrease in the CWB frequency near 50° latitude accounts for the reduction of the effective diffusivity there.

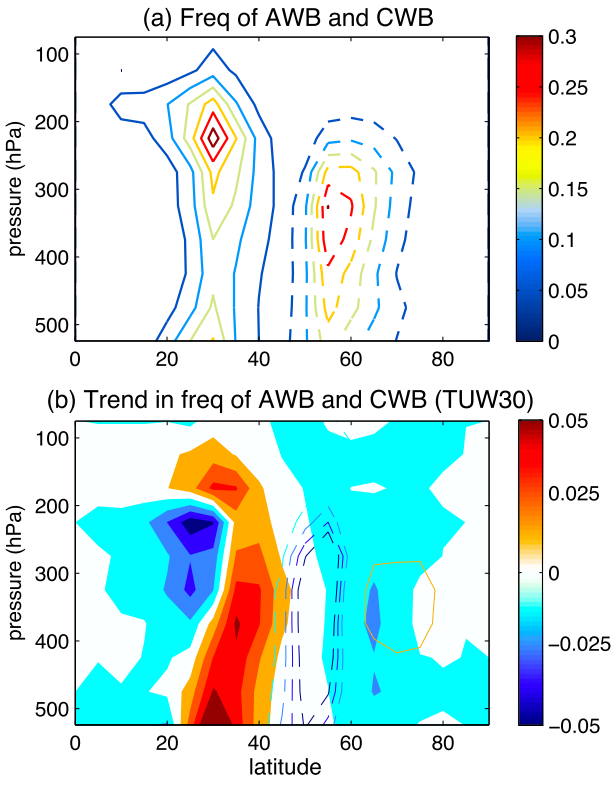

FIG. 9. (a) Climatological latitude–height distribution of the frequency of the AWB and CWB (in unit of fraction of meridians per day). The solid (dashed) contours are for the frequency of the AWB (CWB). (b) As in (a), but for the trend of the frequency of the AWB (shadings) and CWB (contours) over the period days 1–100 in the TUW30 experiment.

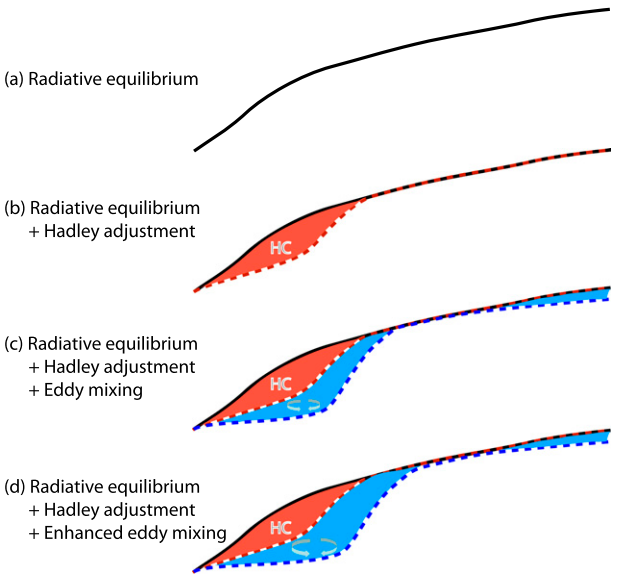

FIG. 10. Schematics for the dynamics processes that shape the meridional structure of the upper tropospheric PV. (a) The monotonic increase of the PV from the equator to pole for a convective–radiative equilibrium state. (b) The PV profile (red dashed curve) resulting from the zonally symmetric Hadley adjustment. (c) The PV profile (blue dashed curve) resulting from both zonally symmetric Hadley adjustment and asymmetric eddy mixing. (d) As in (c), but with a poleward enhancement of the eddy mixing under a global warming–like tropical upper tropospheric heating. The eddy momentum convergence diagnosed from the full model output does align well with the eddy-driven jet near 43°.

Since the heating profile in the TUW30 case is designed to mimic the tropical tropospheric heating associated with global warming, a parallel may be drawn between the results of Fig. 9b and the similar analysis with the simulations by fully coupled climate models. Indeed, the reduction (increase) of the CWB (AWB) frequency at the equatorward (poleward) side of the corresponding climatological distribution is exactly what is ascribed to the changes of upper-level wave breaking statistics due to the greenhouse gas forcing simulated by the French climate models [see upper panels of Fig. 2 in Rivière (2011)].

6. A conceptualization for the circulation response to global warming

The outcome of the hybrid Eulerian–Lagrangian diagnostics in fact provides a simplified depiction of the extratropical circulation response to global warming–related tropical heating. The essential dynamical ingredients of the newly acquired perception through the diagnostics are illustrated schematically in Fig. 10. For the sake of pedagogy, we start with a convective–radiative equilibrium state of the climate, wherein only thermodynamic adjustment is considered and no horizontal communication between the air columns is allowed. The corresponding PV distribution in the upper troposphere is characterized by a smooth, monotonic function of latitude (Fig. 10a). When zonally symmetric adjustment is allowed (as simulated in our zonally symmetric model), the convective–radiative equilibrium state becomes hydrodynamically unstable and gives way to a zonally symmetric Hadley overturning circulation in the tropics, where a quasi-isothermal and quasi-angular momentum-conserving wind is established. The effect of the zonally symmetric adjustment is the homogenization of the PV in the tropical upper troposphere, whereas, in the absence of eddies, the extratropical atmosphere remains in the convective equilibrium state. As such, the contrast between the low tropical PV and the high extratropical PV gives rise to a sharp subtropical PV gradient and a subtropical jet ensues (Fig. 10b). With eddies breaking the zonal symmetry, the effect of subtropical eddy mixing associated with the predominant AWB there works to extend the homogenized area poleward so as to sharpen the PV gradient further and push it and

the corresponding jet poleward (Fig. 10c). This depiction is in exactly the same spirit as the Rossby wave modified Hadley cell in a barotropic model studies by Held and Phillips (1990). Now the jet (if still single) is mixed in its dynamical nature, maintained by both thermal heating and eddy momentum forcing. The single jet in reality generally possesses the similar hybridity in its dynamics. With the jet being viewed as the manifestation of sharp PV gradient, the poleward shift of the jet under the global warming can be simply understood as the result of the enhancement and the poleward encroachment of eddy mixing of PV at the equatorward flank of the mean jet in response to an anomalous tropical upper tropospheric heating associated with the global warming (Fig. 10d).

Interestingly, if one flips the panels in Fig. 10 upside-down and reinterprets the curves as the heights of the 2-PVU (1 PVU = $10^{-6}\,\mathrm{K\,m^2\,kg^{-1}\,s^{-1}}$) surface, a quantity often used for the dynamical tropopause that demarcates the boundary between the well-mixed troposphere and the more stratified stratosphere, the edge of the tropical upper tropospheric homogenization provides a natural definition for the edge of the tropics (e.g., Wilcox et al. 2011). The narrative above about the PV mixing can be readily carried over to account for the poleward expansion of the tropics under the global warming–related tropical thermal forcing. As such, the robust changes in the streamfunction of the Hadley cell, the jet stream, and the tropical width simulated by the Coupled Model Intercomparison Project (CMIP) models under global warming forcing can all be reconciled in light of the altered irreversible PV mixing.

7. Summary

As a companion paper to SCL, the sensitivity and dynamical processes of the response of the atmospheric circulation to tropical upper tropospheric thermal forcing are further investigated from both linear and nonlinear aspects. The results verified a rather counterintuitive finding by the previous studies, that is, a narrow upper tropospheric heating produces characteristically similar eddy flux anomalies and eddy-driven circulation as much broader tropical heating profiles. The reproducibility of this finding by a different dry dynamical core warrants its further investigation for the underlying mechanisms.

Both linear wave refractive index analysis and FAWA budget are performed for the atmospheric response to two tropical heating profiles representing the narrow and broad upper tropospheric warming cases. The linear wave refraction analysis gives an equatorward shift or equatorward enhancement of the momentum forcing for the zonal mean wind for both TUW cases analyzed, while the response with the full eddy adjustment shows a poleward shift of the eddy-driven jet and eddy-driven overturning circulation. The conflicting results between the linear analysis and full nonlinear simulations point to the limitation of the traditional linear WKB theory in guiding our understanding of the eddy feedback in the circulation response to external climate change forcings, such as global warming.

An Eulerian–Lagrangian diagnostic based on equivalent latitude (i.e., corresponding to the area surrounded by PV contours toward to the respective pole) is then applied to the large-size ensemble transient evolutions in response to the heating profiles of interest. It is found that the irreversible downgradient mixing of PV is essential for balancing the anomalous eddy PV flux. Although similar proposition was made in Butler et al. (2011) to account for the wind response to a similarly imposed tropical heating, the nuanced difference revealed by the novel diagnostics here is significant: it is the upward and poleward advance of the effective diffusivity, instead of the change of the PV gradient per se as advocated in Butler et al. (2011), that accounts mostly for the PV dissipation. The assertion with regard to the change of the effective diffusivity is further corroborated by the altered statistics of the upper tropospheric wave breakings. Taken together with Butler et al. (2011), this study helps identify the tropical upper tropospheric heating as one of the robust sources for the poleward shift of the circulation under GHG forcing. Given that the upward shift of latent heating rates and cloud properties are the robust features in the tropical response to the increase of GHG concentrations (Singh and O'Gorman 2012; O'Gorman and Singh 2013), the robustness of the dry dynamical mechanisms identified here with respect to the width of the upper tropospheric heating should contribute to the robust poleward shift of the midlatitude storm track and eddy-driven jet under global warming.

Finally, we end with a cautionary note that the sensitivity to the tropical upper tropospheric warming discussed herein cannot be extended without scrutiny to other distinct circulation regimes, a topic we leave for future investigation.

Acknowledgments. JL acknowledges Edwin Schneider for his internal review when the more primitive version of the manuscript was published as an internal technical report at COLA. The manuscript also benefited substantively from the very constructive comments from Nili Harnik and Gwendal Rivière and a third anonymous reviewer. JL is supported by NSF Grant ATM-1064045 and partly by the Office of Science of the U.S. Department of Energy as part of the Regional and

Global Climate Modeling Program. The Pacific Northwest National Laboratory is operated for DOE by Battelle Memoiral Institute under Contract DE-AC05-76RL01830. LS and GC are supported by NSF Grant ATM-1064079.

REFERENCES

Andrews, D. G., J. R. Holton, and C. Leovy, 1987: *Middle Atmosphere Dynamics.* Academic Press, 489 pp.

Butler, A. H., D. W. J. Thompson, and R. Heikes, 2010: The steady-state atmospheric circulation response to climate change–like thermal forcings in a simple general circulation model. *J. Climate,* **23,** 3474–3496.

——, ——, and T. Birner, 2011: Isentropic slopes, down-gradient eddy fluxes, and the extratropical atmospheric circulation response to tropical tropospheric heating. *J. Atmos. Sci.,* **68,** 2292–2305.

Chang, E. K. M., 1995: The influence of Hadley circulation intensity changes on extratropical climate in an idealized model. *J. Atmos. Sci.,* **52,** 2006–2024.

Charney, J. G., and P. G. Drazin, 1961: Propagation of planetary-scale disturbances from the lower into the upper atmosphere. *J. Geophys. Res.,* **66** (1), 83–109.

Chen, G., J. Lu, and D. M. W. Frierson, 2008: Phase speed spectra and the latitude of surface westerlies: Interannual variability and global warming trend. *J. Climate,* **21,** 5942–5959.

——, ——, and L. Sun, 2013: Delineating the eddy–zonal flow interaction in the atmospheric circulation response to climate forcing: Uniform SST warming. *J. Atmos. Sci.,* **70,** 2214–2233.

Ferrari, R., and M. Nikurashin, 2010: Suppression of eddy diffusivity across jets in the Southern Ocean. *J. Phys. Oceanogr.,* **40,** 1501–1519.

Frierson, D. M. W., J. Lu, and G. Chen, 2007: The width of the Hadley cell in simple and comprehensive general circulation models. *Geophys. Res. Lett.,* **34,** L18804, doi:10.1029/2007GL031115.

Haigh, J. D., M. Blackburn, and R. Day, 2005: The response of tropospheric circulation to perturbations in lower-stratospheric temperature. *J. Climate,* **18,** 3672–3685.

Harnik, N., and R. S. Lindzen, 2001: The effect of reflecting surface on the vertical structure and variability of stratospheric planetary waves. *J. Atmos. Sci.,* **58,** 2872–2894.

——, R. Seager, N. Naik, M. Cane, and M. Ming, 2010: The role of linear wave refraction in the transient eddy–mean flow response to tropical Pacific SST anomalies. *Quart. J. Roy. Meteor. Soc.,* **136,** 2132–2146.

Haynes, P. H., and E. F. Shuckburgh, 2000: Effective diffusivity as a diagnostic of atmospheric transport: 2. Troposphere and lower stratosphere. *J. Geophys. Res.,* **105** (D18), 22 795–22 810.

——, D. A. Poet, and E. F. Shuckburgh, 2007: Transport and mixing in kinematic and dynamically consistent flows. *J. Atmos. Sci.,* **64,** 3640–3651.

Held, I. M., and A. Y. Hou, 1980: Nonlinear axially symmetric circulations in a nearly inviscid atmosphere. *J. Atmos. Sci.,* **37,** 515–533.

——, and P. J. Phillips, 1990: A barotropic model of the interaction between the Hadley cell and Rossby wave. *J. Atmos. Sci.,* **47,** 856–869.

——, and M. J. Suarez, 1994: A proposal for the intercomparison of the dynamical cores of atmospheric general circulation models. *Bull. Amer. Meteor. Soc.,* **75,** 1825–1830.

Hoskins, B. J., and D. J. Karoly, 1981: The steady linear response of a spherical atmosphere to thermal and orographic forcing. *J. Atmos. Sci.,* **38,** 1179–1196.

Kang, S., and J. Lu, 2012: Expansion of the Hadley cell under global warming: Winter versus summer. *J. Climate,* **25,** 8387–8393.

Kidston, J., G. K. Vallis, S. M. Dean, and J. A. Renwick, 2011: Can the increase in the eddy length scale under global warming cause the poleward shift of the jet streams? *J. Climate,* **24,** 3764–3780.

Kim, H., and S. Lee, 2001: Hadley cell dynamics in a primitive equation model. Part II: Nonaxisymmetric flow. *J. Atmos. Sci.,* **58,** 2859–2871.

Kushner, P. J., and L. M. Polvani, 2004: Stratosphere–troposphere coupling in a relatively simple AGCM: The role of eddies. *J. Climate,* **17,** 629–639.

Lorenz, D. J., and E. T. DeWeaver, 2007: Tropopause height and zonal wind response to global warming in the IPCC scenario integrations. *J. Geophys. Res.,* **112,** D10119, doi:10.1029/2006JD008087.

Lu, J., G. A. Vecchi, and T. Reichler, 2007: Expansion of the Hadley cell under global warming. *Geophys. Res. Lett.,* **34,** L06805, doi:10.1029/2006GL028443.

——, G. Chen, and D. M. W. Frierson, 2008: Response of the zonal mean atmospheric circulation to El Niño versus global warming. *J. Climate,* **21,** 5835–5851.

——, ——, and ——, 2010: The position of the midlatitude storm track and eddy-driven westerlies in aquaplanet AGCMs. *J. Atmos. Sci.,* **67,** 3984–4000.

Marshall, J., E. Shuckburgh, H. Jones, and C. Hill, 2006: Estimates and implications of surface eddy diffusivity in the Southern Ocean derived from tracer transport. *J. Phys. Oceanogr.,* **36,** 1806–1821.

Matsuno, T., 1970: Vertical propagation of stationary planetary waves in the winter Northern Hemisphere. *J. Atmos. Sci.,* **27,** 871–883.

Methven, J., 2013: Wave activity for large-amplitude disturbances described by the primitive equations on the sphere. *J. Atmos. Sci.,* **70,** 1616–1630.

Nakamura, N., 1996: Two-dimensional mixing, edge formation, and permeability diagnosed in an area coordinate. *J. Atmos. Sci.,* **53,** 1524–1537.

——, and A. Solomon, 2010: Finite-amplitude wave activity and mean flow adjustments in the atmospheric general circulation. Part I: Quasigeostrophic theory and analysis. *J. Atmos. Sci.,* **67,** 3967–3983.

——, and D. Zhu, 2010: Finite-amplitude wave activity and diffusive flux of potential vorticity in eddy–mean flow interaction. *J. Atmos. Sci.,* **67,** 2701–2716.

O'Gorman, P. A., and M. S. Singh, 2013: Vertical structure of warming consistent with an upward shift in the middle and upper troposphere. *Geophys. Res. Lett.,* **40,** 1838–1842, doi:10.1002/grl.50328.

Perlwitz, J., and N. Harnik, 2003: Observational evidence of a stratospheric influence on the troposphere by planetary wave reflection. *J. Climate,* **16,** 3011–3026.

Plumb, R. A., and R. Ferrari, 2005: Transformed Eulerian-mean theory. Part I: Nonquasigeostrophic theory for eddies on a zonal mean flow. *J. Phys. Oceanogr.,* **35,** 165–174.

Ren, H.-L., F.-F. Jin, J.-S. Kug, and L. Gao, 2011: Transformed eddy-PV flux and positive synoptic eddy feedback onto low-frequency flow. *Climate Dyn.,* **36,** 2357–2370, doi:10.1007/s00382-010-0913-0.

Rivière, G., 2009: Effect of latitudinal variations in low-level baroclinicity on eddy life cycles and upper-tropospheric wave-breaking processes. *J. Atmos. Sci.,* **66,** 1569–1592.

——, 2011: A dynamical interpretation of the poleward shift of the jet streams in global warming scenarios. *J. Atmos. Sci.,* **68,** 1253–1272.

Satoh, M., 1994: Hadley circulations in radiative–convective equilibrium in an axially symmetric atmosphere. *J. Atmos. Sci.,* **51,** 1947–1968.

Scheff, J., and D. Frierson, 2012: Twenty-first-century multimodel subtropical precipitation declines are mostly midlatitude shifts. *J. Climate,* **25,** 4330–4347.

Schneider, E. K., 1977: Axially symmetric steady-state models of the basic state for instability and climate studies. Part II: Nonlinear calculations. *J. Atmos. Sci.,* **34,** 280–296.

Seager, R., N. Harnik, Y. Kushnir, W. A. Robinson, and J. Miller, 2003: Mechanisms of hemispherically symmetric climate variability. *J. Climate,* **16,** 2960–2978.

——, and Coauthors, 2007: Model projection of an imminent transition to a more arid climate in southwestern North America. *Science,* **316,** 1181–1184, doi:10.1126/science.1139601.

Singh, M. S., and P. A. O'Gorman, 2012: Upward shift of the atmospheric general circulation under global warming: Theory and simulations. *J. Climate,* **25,** 8259–8276.

Sun, L., J. Lu, and G. Chen, 2013: Sensitivities and mechanisms of the zonal mean atmospheric circulation response to tropical warming. *J. Atmos. Sci.,* **70,** 2487–2504.

Tanaka, D., T. Iwasaki, S. Uno, M. Ujiie, and K. Miyazaki, 2004: Eliassen–Palm flux diagnosis based on isentropic representation. *J. Atmos. Sci.,* **61,** 2370–2383.

Wilcox, L. J., B. J. Hoskins, and K. P. Shine, 2011: A global blended tropopause based on ERA data. Part II: Trends and tropical broadening. *Quart. J. Roy. Meteor. Soc.,* **138,** 576–584.

Williams, G. P., 2006: Circulation sensitivity to tropopause height. *J. Atmos. Sci.,* **63,** 1954–1961.

Wu, Y., R. Seager, M. Ting, N. Naik, and T. Shaw, 2012: Atmospheric circulation response to an instantaneous doubling of carbon dioxide. Part I: Model experiments and transient thermal response in the troposphere. *J. Climate,* **25,** 2862–2879.

——, ——, T. A. Shaw, M. Ting, and N. Naik, 2013: Atmospheric circulation response to an instantaneous doubling of carbon dioxide. Part II: Atmospheric transient adjustment and its dynamics. *J. Climate,* **26,** 918–935.